Check for updates

Proceedings of the ASME 2023 Heat Transfer Summer Conference
HT2023
July 10-12, 2023, Washington, DC

HT2023-106873

Downloaded from http://asmedigitalcollection.asme.org/HT/proceedings-pdf/HT2023/87165/V001T03A002/7042647/v001t03a002-ht2023-106873.pdf by Rochester Institute Of Technology, Michael Medlar on 07 November 2023

ELECTRON-PHONON INTERACTIONS FOR NANOSCALE ENERGY TRANSPORT SIMULATIONS IN SEMICONDUCTOR DEVICES

Michael P. Medlar, Edward C. Hensel
Rochester Institute of Technology, Rochester, NY, USA

ABSTRACT

An ideal semiconductor device would permit unimpeded flow of electrons from its source to its drain in a fashion that can be switched on and off by its gate at high frequency. Electron flow through real semiconductor devices is impeded by interactions with the crystalline structure of the material. Electrons which interact with the crystal may generate phonons which manifest as thermal energy generation and degrade real device performance from its ideal limit. Accurate simulation of electron-phonon interactions cannot rely on the traditional continuum assumption because of the reduced length and time scales of modern semiconductor devices. Allowable electron-phonon interactions are constrained by the conservation of energy and momentum. Direct enforcement of the conservation laws is achieved through computation of an interaction table that contains thousands of rows each of which representing a conservative interaction. The rows represent both phonon and electron creation and annihilation. The electron and phonon wavevector space is discretized into 65,856 elements and the table is computed by searching the discretized wavevector space for electron and phonon states that first satisfy the conservation of momentum. Subsequently, these states are compared against the conservation of energy using the phonon and electron dispersion relations. Anisotropic phonon dispersion relations were calculated using a second nearest neighbor lattice dynamics approach with interatomic force constants from Density Functional Theory. Electron dispersion relations were computed using an empirical pseudopotential approach. This method was demonstrated for computation of electron-phonon interactions in silicon, resulting in an initial interaction table containing approximately 58,000 interactions. Computation of the electron energies associated with the first conduction band in an anisotropic manner illustrate reasonable agreement with published work. The interaction densities show similar functionality relative to the electron-phonon interaction rate predictions and phonon generation rates from published literature. The interaction table directly enforces the conservation laws on all electron-phonon interactions and the interaction table approach can be used for high fidelity electron-phonon simulations to quantify the mechanism, rate, and location of thermal losses arising at the nanoscale.

Keywords: Electron-Phonon Interactions, Interaction Table, Nanoscale Thermal Transport

NOMENCLATURE

α	Atom number identifier
$\hbar$	Modified Plank's constant
τ	Atom position vector
ω	Angular frequency
Ω	Crystal volume
ψ	State vector
E	Energy
G	Reciprocal lattice vector
k	Phonon wavevector
m	Electron mass
N	Number of atoms
q	Electron wavevector
r	Position vector
s	Phonon polarization
u	Crystal periodic function
V	Potential

1. INTRODUCTION

Electron-phonon interactions are the source of thermal energy generation in semiconductor devices and impact both thermal and electrical performance. Scattering by phonons is one of the most important processes in charge transport for semiconductors as it limits electron velocity [1] and ON-current [2, 3]. Accurate prediction of electron-phonon interactions is required for high fidelity device simulations.

Prediction of electron-phonon interactions with the methodology presented with this work offers serval advantages that lead to

Copyright © 2023 by ASME

higher fidelity electron-phonon simulations. First, anisotropic electron and phonon dispersion relations are used to represent the electron and phonon states. Some works, like Rowlette and Goodson [4], employ simplified analytic models for electron dispersion and quadratic relations for the phonon dispersion. The use of anisotropic dispersion relations for both the phonon [5] and electron population results in a more detailed computation of the allowed interactions subject to conservation rules. Second, compiling electron-phonon interactions within a pre-computed table allows direct enforcement of the conservation laws in every electron-phonon scattering interaction. Simulation methods like those of the Monte Carlo technique of Wu et al [6] for phonon transport delete phonons from the simulation domain after a scattering event and new ones are introduced randomly from the equilibrium distribution. This does not result in conservation of momentum or energy in an individual scattering event. And lastly, knowledge of all the interactions available for phonons and electrons allows for updating the electron and phonon populations with the actual number of phonons or electrons involved in individual scattering events based on relative probabilities of interaction. This eliminates the need for scaling factors and random numbers typical of Monte Carlo simulations [1, 7, 8] resulting in higher fidelity simulations.

2. METHODS

2.1 Theory

Silicon is the most common semiconductor material used in commercial devices today. The crystal structure of silicon dictates the dispersion relationships for phonons and electrons that have a direct effect on allowable interactions. Dispersion relations for phonons have been computed with prior work using the lattice dynamics approach with interatomic force constants up to second nearest neighbors from Density Functional Theory and documented in [5]. Electron dispersion relations are computed with the empirical pseudopotential approach [9, 10]. This approach relies on solution of an effective one electron Schrodinger equation as shown in equation 1,

$$\left[\frac{-\hbar^2}{2m}\nabla^2 + V^{lat}\right]|\psi\rangle = E|\psi\rangle \ , \tag{1}$$

where $\hbar$ is modified planks constant, m is the electron mass, $|\psi\rangle$ is the electron wavefunction, V^{lat} is the lattice potential, and E is the energy. As the lattice potential is periodic, the electron wavefunctions can be expanded using Bloch's theorem [10].

$$|\psi\rangle = \frac{1}{\Omega^{1/2}} e^{iq\cdot r} \sum_G u_{qG} e^{iG\cdot r} \ , \tag{2}$$

where Ω is the crystal volume, q is the wavevector, r is position vector, u_{qG} is a crystal periodic function, and G is a reciprocal lattice vector. Upon simplification and manipulation, equation 1 becomes equation 3.

$$\left[\frac{-\hbar^2}{2m}|q+G|^2 - E(q)\right] u_{qG} + \sum_{G'} V_{GG'} u_{qG} = 0, \tag{3}$$

where $V_{GG'}$ is the Fourier transform of the lattice potential. Solution of the Schrodinger equation with these simplifications relies on an intractable number of plane waves to accurately represent both the core wavefunctions and valance wavefunctions, so approximation is required. With the pseudopotential approach, the modified lattice potential ($V_{GG'}$) is transformed to represent the effective potential felt by just the valance electrons. This implies that the solutions only give results for valance wavefunctions and are valid only outside the core region of the ions. Typically, the pseudopotential is expressed as the product of a piece depending on the atomic locations in the unit cell and a form factor accounting for the shape of the atomic potential as is shown in equation 4.

$$V_{GG'} = \frac{1}{N_\alpha} \sum_\alpha e^{-i(G-G')\cdot\tau_\alpha} V_{G-G'} \ , \tag{4}$$

where G and G' are reciprocal lattice vectors, τ_α is the position vector to the location of atom α, N_α is the number of atoms in the unit cell, and $V_{G-G'}$ is the form factor. With the empirical form of this approach, adjustable parameters within the form factor are tuned to reproduce binding properties of the crystal and band structure features that match experimental data [10]. Considering the two atom basis of silicon with the origin directly between the two identical atoms and the atomic locations given by $\pm\tau_\alpha = \pm\frac{a}{8}(1,1,1)$, the pseudopotential becomes equation 5.

$$V_{GG'} = V_{G-G'}[cos((G-G')\cdot\tau_\alpha)] \ , \tag{5}$$

A limited number of form factors are required to show good agreement between the band structure and experimental data (energy band splitting). The values used for this work are that given by Cohen and Bergstresser [9] and shown in Table 1 labeled by the square of the difference in reciprocal lattice vectors.

TABLE 1: FORM FACTOR PARAMETERS IN UNITS OF RYDBERGS

$(G-G')^2$	$V_{G-G'}$
3	-0.21
8	0.04
11	0.08

Phonon and electron dispersion relations allow prediction of possible electron-phonon interactions. In the inelastic interaction, an electron emits a phonon as it transitions to a lower energy state or an electron absorbs a phonon to reach a higher energy state. This interaction is schematically illustrated with Fig. 1 [11].

Copyright © 2023 by ASME

Downloaded from http://asmedigitalcollection.asme.org/HT/proceedings-pdf/HT2023/87165/V001T03A002/7042647/v001t03a002-ht2023-106873.pdf by Rochester Institute Of Technology, Michael Medlar on 07 November 2023

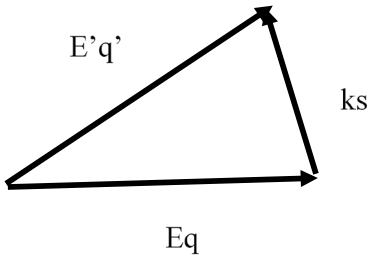

FIGURE 1: ELECTRON PHONON INTERACTION ILLUSTRATION. THE VECTORS LABELED E'q' AND Eq REPRESENT DIFFERENT ELECTRON STATES AND THE VECTOR LABELED ks REPRESENTS A PHONON [11].

Interactions are constrained to satisfy the conservation of momentum and energy as illustrated with equations 6 and 7.

$$q + k = q' + G, \tag{6}$$

$$\mathrm{E}(\mathrm{q}) + \hbar\omega(\mathrm{k}) = \mathrm{E}'(\mathrm{q}'), \tag{7}$$

where q and q' are electron wavevectors, k is a phonon wavevector, G is a reciprocal lattice vector, E and E' are electron energies, and ω is the phonon frequency.

2.2 Implementation

Computation of allowable electron-phonon scattering interactions relies on discretization of the wavevector space. The first octant of the First Brillouin Zone (FBZ) was discretized with a uniform mesh of 14x14x14 elements in the K_x, K_y, and K_z directions to produce 1,372 wavevector states. A search scheme applied to the discretized FBZ is implemented in which the wavevector of the centroid of each element is compared to every other one in the FBZ to determine all of the combinations that conserve momentum. Momentum conservation is ensured up to the addition of a reciprocal lattice vector (G) and both normal and Umklapp processes are considered. If an interaction is deemed to satisfy momentum conservation (equation 6), it is then checked for energy conservation using the results of the computed dispersion relations and equation 7 (up to a pre-specified relative tolerance). The interactions that are deemed to meet the criteria of equations 6 and 7 are included in the electron-phonon interaction table.

3. RESULTS AND DISCUSSION

The lattice dynamics formulation used for computation of phonon dispersion relations documented in [4] resulted in anisotropic prediction of dispersion relations that showed good agreement with experimental data in high symmetry directions.

Prediction of the first conduction band energies using the empirical pseudopotential method are illustrated over 1/8 of the FBZ in Fig. 2.

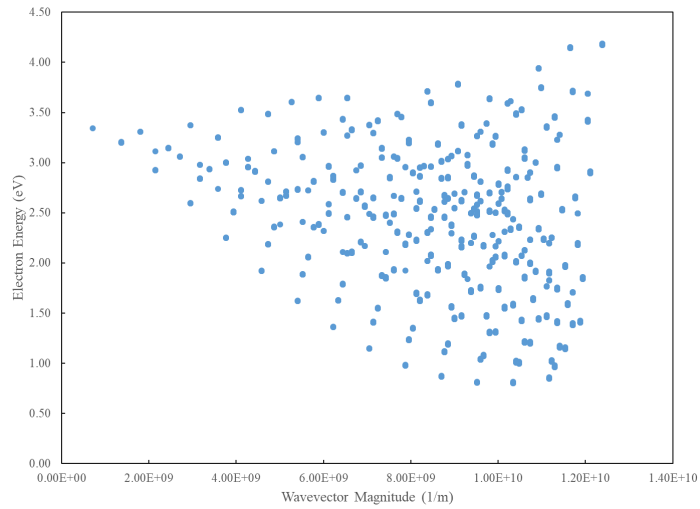

FIGURE 2: ELECTRON FIRST CONDUCTION BAND ENERGIES ACROSS 1/8 OF THE FIRST BRILLOUIN ZONE.

Traditional models of the first conduction band rely only on high symmetry directions of the crystalline structure, whereas Fig. 2 accounts for the full anisotropic nature of the silicon crystal structure. This provides a full accounting for all energy and momentum conditions of the discrete electron states that are available to interact with the crystalline structure and partner with phonons to dissipate thermal energy.

Fig. 3 shows a prior prediction from Hamaguchi [12] of the first conduction band energy vs. wavevector magnitude along the high symmetry direction L-G-X. Overlaid on Fig. 3 is our fully anisotropic model limited to the same symmetry direction.

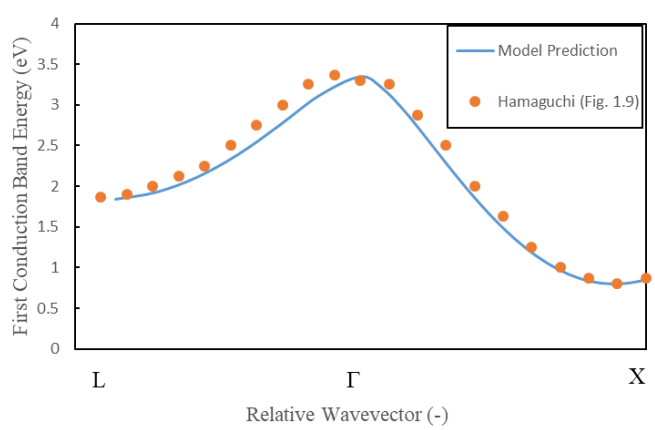

FIGURE 3: ELECTRON FIRST CONDUCTION BAND ENERGIES FOR CURRENT MODEL PREDICTIONS COMPARED AGAINST FIG. 1.9 OF HAMAGUCHI [12].

The anisotropic model compares well against previously published results. Conversely, the anisotropic electron model is not limited to planes of high symmetry and enables conservation of momentum and energy with all possible phonon partners.

Downloaded from http://asmedigitalcollection.asme.org/HT/proceedings-pdf/HT2023/87165/V001T03A002/7042647/v001t03a002-ht2023-106873.pdf by Rochester Institute Of Technology, Michael Medlar on 07 November 2023

Copyright © 2023 by ASME

The anisotropic electron model, equations 1-5 presented in Fig. 2, was used in conjunction with the anisotropic phonon model, previously published in [5], to generate a scattering table as described by equations 6 and 7. The results are illustrated with Fig. 4.

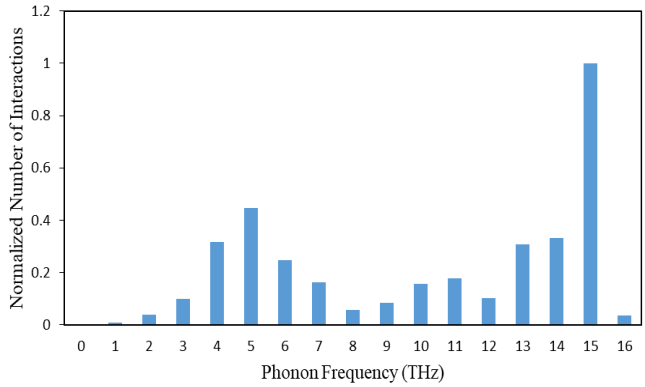

FIGURE 4: NORMALIZED NUMBER OF ELECTRON-PHONON INTERACTIONS PLOTTED AS A FUNCTION OF PHONON FREQUENCY.

The Fig. 4 results match the limited one-dimensional investigation previously documented by Medlar and Hensel [13]. In addition, the trends illustrated with Fig. 4 show similar functionality relative to both the electron-phonon scattering rate predictions of Liao et al. [14] and the phonon generation rates of Rowlette and Goodson [4].

The results illustrate that electrons preferentially scatter with phonon of different types. For example, the interactions above approximately 12 THz, which are a dominant source of thermal energy generation, represents interactions between electrons and optical phonons. The secondary peak centered at 5 THz represents interactions between electrons and acoustic phonons. Optical phonons generated from electron scattering have relatively low group velocities but subsequently decay into two acoustic phonons through three-phonon scattering. Thus, designing heat sinks to dissipate energy generation reflected in electron-phonon scattering should account for the spectrum of generated phonons. Spectrum focused heat removal has the possibility to permit semiconductor devices to be operated at higher frequency than can be achieved today due to present thermal limitations.

4. CONCLUSION

Computation of anisotropic electron dispersion relations and a search of the wavevector space for conservative interactions allowed for development of an electron-phonon interaction table. This method provides the basis for development of a full electron-phonon scattering algorithm that will directly enforce the conservation laws in any given interaction and redistribute phonons and electrons by exact amounts relative to the likelihood of specific interactions thus improving modeling fidelity.

REFERENCES

[1] Pop, E., 2014, "Monte Carlo Transport and Heat Generation in Semiconductors," Annual Review of Heat Transfer, 17(N/A), pp. 385-423.

[2] Rhyner, R., and Luisier, M., 2014, "Atomistic Modeling of Coupled Electron-Phonon Transport in Nanowire Transistors," Physical review. B, Condensed matter and materials physics, 89(23).

[3] Rhyner, R., and Luisier, M., 2016, "Minimizing Self-Heating and Heat Dissipation in Ultrascaled Nanowire Transistors," Nano letters, 16(2), pp. 1022-1026.

[4] Rowlette, J. A., and Goodson, K. E., 2008, "Fully Coupled Nonequilibirum Electron-Phonon Transport in Nanometer-Scale Silicon Fets," IEEE Transactions on Electron Devices, 55(1).

[5] Medlar, M. P., and Hensel, E. C., 2020, "Validation of an Enhanced Dispersion Algorithm for Use with the Statistical Phonon Transport Model," Proc. ASME 2020 Heat Transfer Summer Conference, ASME 2020 Heat Transfer Summer Conference.

[6] Wu, R., Hu, R., and Luo, X., 2016, "First-Principle-Based Full-Dispersion Monte Carlo Simulation of the Anisotropic Phonon Transport in the Wurtzite Gan Thin Film," Journal of Applied Physics, 119(14), pp. 145706.

[7] Wong, B. T., Francoeur, M., and Pinar Mengüç, M., 2011, "A Monte Carlo Simulation for Phonon Transport within Silicon Structures at Nanoscales with Heat Generation," International journal of heat and mass transfer, 54(9), pp. 1825-1838.

[8] Mohamed, M., Aksamija, Z., Vitale, W., Hassan, F., Park, K.-H., and Ravaioli, U., 2014, "A Conjoined Electron and Thermal Transport Study of Thermal Degradation Induced During Normal Operation of Multigate Transistors," IEEE Transactions on Electron Devices, 61(4), pp. 976-983.

[9] Cohen, M. L., and Bergstresser, T. K., 1966, "Band Structures and Pseudopotential Form Factors for Fourteen Semiconductors of the Diamond and Zinc-Blende Structures," Physical review, 141(2), pp. 789-796.

[10] Fischetti, M. V., Vandenberghe, W. G., and Springerlink, 2016, Advanced Physics of Electron Transport in Semiconductors and Nanostructures, Springer International Publishing, Cham.

[11] Lundstrom, M., 2011, Fundamentals of Carrier Transport (2nd Edition), Cambridge University Press, Cambridge, GBR.

[12] Hamaguchi, C., 2001, Basic Semiconductor Physics, Springer, New York;Berlin;.

[13] Medlar, M., and Hensel, E., 2022, "An Enhanced Statistical Phonon Transport Model for Nanoscale Thermal Transport," J of Heat Transfer - Transactions of the ASME.

[14] Liao, B., Qiu, B., Zhou, J., Huberman, S., Esfarjani, K., Chen, G., and Energy Frontier Research Centers . Solid-State Solar-Thermal Energy Conversion, C., 2015, "Significant Reduction of Lattice Thermal Conductivity by the Electron-Phonon Interaction in Silicon with High Carrier Concentrations: A First-Principles Study," Physical Review Letters, 114(11).

Downloaded from http://asmedigitalcollection.asme.org/HT/proceedings-pdf/HT2023/87165/V001T03A002/7042647/v001t03a002-ht2023-106873.pdf by Rochester Institute Of Technology, Michael Medlar on 07 November 2023

Copyright © 2023 by ASME